NANO LETTERS

2007
Vol. 7, No. 10
2942−2950

Synthesis and Micrometer-Scale Assembly of Colloidal CdSe/CdS Nanorods Prepared by a Seeded Growth Approach

Luigi Carbone,[†,‡] Concetta Nobile,[†,‡] Milena De Giorgi,[‡] Fabio Della Sala,[‡] Giovanni Morello,[‡] Pierpaolo Pompa,[‡] Martin Hytch,[§] Etienne Snoeck,[§] Angela Fiore,[‡] Isabella R. Franchini,[‡] Monica Nadasan,[‡] Albert F. Silvestre,[‡] Letizia Chiodo,[‡] Stefan Kudera,[‡] Roberto Cingolani,[‡] Roman Krahne,[‡] and Liberato Manna*[,‡]

NNL-National Nanotechnology Laboratory of CNR-INFM and IIT Research Unit, via per Arnesano, km 5, 73100 Lecce, Italy, and CEMES-CNRS, 29 rue Jeanne Marvig, B.P. 94347, F-31055 Toulouse Cedex, France

Received July 20, 2007

ABSTRACT

Key limitations of the colloidal semiconductor nanorods that have been reported so far are a significant distribution of lengths and diameters as well as the presence of irregular shapes produced by the current synthetic routes and, finally, the poor ability to fabricate large areas of oriented nanorod arrays. Here, we report a seeded-growth approach to the synthesis of asymmetric core–shell CdSe/CdS nanorods with regular shapes and narrow distributions of rod diameters and lengths, the latter being easily tunable up to 150 nm. These rods are highly fluorescent and show linearly polarized emission, whereby the emission energy depends mainly on the core diameter. We demonstrate their lateral alignment as well as their vertical self-alignment on substrates up to areas of several square micrometers.

Ordered assemblies of nanorods are important both in fundamental research, as they present new systems on which chemical and physical interactions among nanocrystals can be investigated, and for practical applications, as they provide the basis to the engineering of new materials and the fabrication of devices. Significant progress has been made recently both on the synthesis of nanorods of different materials[1−3] as well as on understanding and mastering their assembly.[4,5] This can be mediated for instance by external fields,[6−10] by interparticle interactions as well as rod solubility in a binary solvent/nonsolvent liquid mixture,[11−13] by controlling the rod interfacial energy, by slow solvent evaporation on a liquid−solid−air interface,[14] by solvent fluidics and the presence of liquid−air interface in the deposition of a lyotropic phase from a drying solution,[15] by a Langmuir−Blodgett approach,[16] or by unidirectional alignment through attachment of nanorods to the surface of a single cleaved semiconductor monolayer.[17] Important requirements for organizing nanorods in ordered close-packed arrays over significantly large areas are, however, a high homogeneity of shapes and, in the case of alignment assisted by external biases, the ability of nanorods to respond to such biases effectively.

We have developed a new, seeded-type growth approach to fabricate colloidal nanorods, which we have successfully applied to the synthesis of mixed CdSe/CdS nanorods with narrow distributions of rod lengths and diameters. Our CdSe/CdS nanorods present the appealing characteristics of strong and tunable light emission from green to red, they spontaneously self-assemble on substrates, and can be easily organized in close-packed ordered arrays over large areas. The synthesis is based on the co-injection of appropriate precursors and preformed spherical CdSe nanocrystal seeds (nearly monodisperse in size) in a reaction flask that contains a mixture of hot surfactants suited for the anisotropic growth of CdS nanocrystals. In a typical synthesis of nanorods reported in this work, CdO is decomposed in the presence of a mixture of trioctylphosphine oxide, hexylphosphonic acid, and octadecylphosphonic acid in relative ratios that have been carefully optimized (see Supporting Information for details). The resulting solution is heated to 350−380 °C (depending

* Corresponding author. E-mail: liberato.manna@unile.it. Telephone: +39 0832 298 207. Fax: +39 0832 298 238.
[†] These authors have contributed equally to this work.
[‡] NNL-National Nanotechnology Laboratory of CNR-INFM and IIT Research Unit.
[§] CEMES-CNRS.

10.1021/nl0717661 CCC: $37.00
Published on Web 09/11/2007

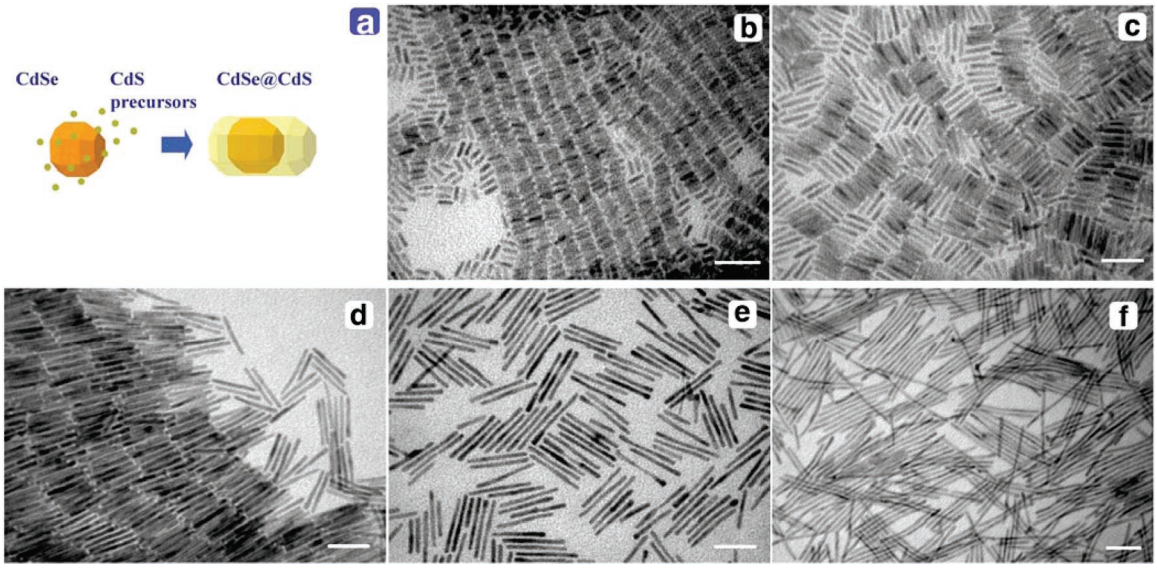

Figure 1. Evaporation-mediated self-assembly of CdSe/CdS nanorods prepared by seeded growth. (a) Sketch of the seeded growth approach. (b−f) Transmission electron micrographs of self-assembled CdSe/CdS nanorods. As soon as the solvent, in which the CdSe/CdS are dissolved (toluene), is allowed to evaporate from the grid on which the drop of solution is deposited, the nanorods start self-assembling. Short aspect ratio (rod length/rod diameter, AR) rods (b−d) tend to form locally ordered 2D smectic phases, while longer rods tend to form either disordered assemblies, ribbons, or locally ordered 2D nematic phases. A similar AR dependence on the assembly was reported for instance for Ag and Au nanorods[4] and pencil-shaped CoO nanocrystals.[20] Average rod diameter and length, as determined by HRTEM, are respectively: (b) 4.9 ± 0.7 nm and 19 ± 1 nm; (c) 4.2 ± 0.4 nm and 35 ± 2 nm; (d) 3.9 ± 0.2 nm and 53 ± 4 nm; (e) 3.8 ± 0.3 nm and 70 ± 4 nm; (f) 3.8 ± 0.3 nm and 111 ± 10 nm. The conditions at which the various nanorod samples are grown are reported in Table 1 of the Supporting Information. In general, the mean rod diameter is dictated not only by the diameter of the seeds but also by the growth temperature, which can control the thickness of the shell (higher temperatures promote the formation of a thicker shell). The rod length on the other hand can be varied not only by the amount of precursors and/or seeds added but also by the growth temperature and/or reaction time. Also, the amount and the size of the added seeds has an influence on the overall length of the rods. Large seeds, for instance, tend to promote the formation of short (and fat) rods (b), while small seeds tend to form long (and thin) rods (f). All scale bars are 50 nm long.

on the synthesis) under inert atmosphere. Separately, a solution is prepared by dissolving sulfur in trioctylphosphine and by adding to it either CdS or CdSe nanocrystals (previously prepared, purified, and solubilized in TOP). This solution is quickly injected in the flask, after which the temperature of the flask is allowed to recover to its pre-injection value and the synthesis is kept running for several minutes before stopping it by removing the heating mantle. Immediately after injection, CdS starts growing preferentially on the CdSe seeds rather than forming separate nuclei in solution because the activation energy for heterogeneous nucleation is much lower than that for homogeneous nucleation.[18] As the homogeneous nucleation is bypassed by the presence of the seeds, all nanocrystals undergo almost identical growth conditions and therefore they maintain a narrow distribution of lengths and diameters during their evolution. The synthesis is rather flexible, as there are various parameters that can be tuned in order to control the morphology of the resulting nanorods such as the diameter of the seeds, the growth temperature, and the amount of precursors and seeds added (see Figure 1). When no CdSe seeds are co-injected, CdS nanorods start nucleating only several seconds after the injection, and the final sample is characterized by large distributions of rod lengths and diameters. Also, the range of aspect ratios (rod length/rod diameter, ARs) of the rods attainable with the present synthesis (up to 30:1) is much wider than that attainable with the synthesis scheme reported by Talapin and co-workers for asymmetric CdSe/CdS core−shell nanorods, which was based on an extension of the traditional synthesis of core−shell nanocrystals (for which the maximum AR reported was 4:1).[19] The power of the seeded-growth approach carried out at high temperatures in suitable surfactant mixtures is therefore that large AR rods can be synthesized that still preserve regular shapes and show no tendency to aggregate, all features that are not achievable with lower-temperature shell-growth approaches.

A key issue of this type of synthesis approach is whether the original seed is preserved in the final rod structure and also which is the location of the seed along the rod. This can be partly elucidated by carrying out geometric phase analysis (GPA),[21] which is a quantitative high-resolution transmission electron microscopy (HRTEM) technique. It allows detection of variations in the periodicities of the HRTEM contrast via analysis of the local components in the Fourier transform of the image. Possible deformations and strains of the 2D-projected lattice can be deduced with respect to an "unstrained" area within the HRTEM image taken as reference. This method was applied to HRTEM images recorded on CdSe/CdS nanorods (Figure 2a) and also on "CdS-only" nanorods that were grown using spherical CdS seeds (Figure 2b). The images were taken on a 200 kV TEM-FEG microscope (F-20 FEI) fitted with a spherical aberration corrector (CEOS). In the corresponding "mean dilatation" (i.e., the average of the 2D lattice deformation) image of a CdSe/CdS nanorod of Figure 2c,

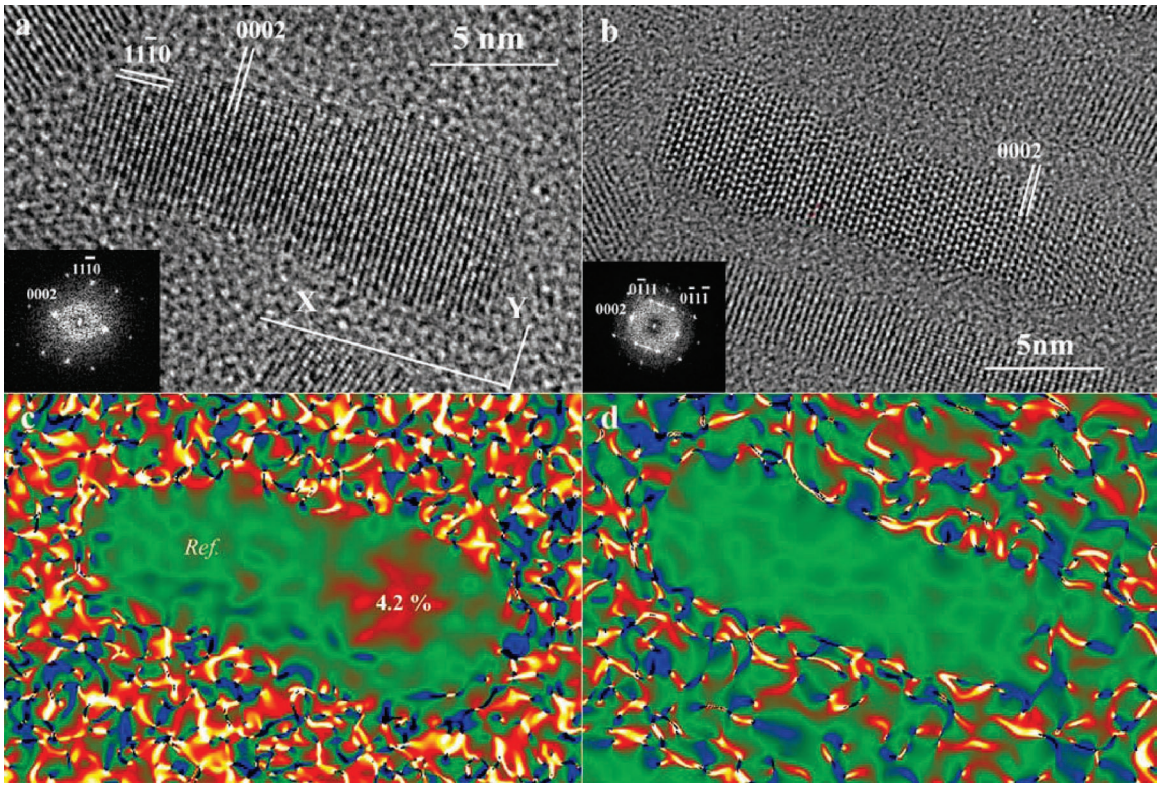

Figure 2. Structural analysis of seeded-grown nanorods. HRTEM images of nanorods grown using either CdSe (a) or CdS (b) as seeds. The nanorods show little occurrence of stacking faults over the entire structure due to the high temperature at which they are grown. (c,d) Corresponding "mean dilatation" images. This technique allows a mean dilatation mapping from high-resolution electron microscope images or indeed any type of lattice image. It uses a color scale for displaying variation in the periodicity of the HRTEM contrast. Areas of the same color are regions with the same periodicity. The mean dilatation image of the CdSe/CdS rod (c) shows an area with lattice parameters altered by 4.2% with respect to the reference area, situated at the opposite tip of the rod. For comparison, the same analysis is performed on "CdS-only" rods, and no variation of the lattice parameters over the whole length of the nanorod can be observed (d).

for instance, it is possible to recognize at the right side of the nanorod a region with a lattice constant different from that of a reference area at the opposite tip. This region should correspond to the original CdSe seed, and this is supported by the quantitative measurement of the relative dilatation (4.2%), which is almost equal to the misfit between bulk CdS and CdSe (i.e., +4%). As a control, the deformation image of a CdS-only rod (Figure 2d) shows an undistorted lattice across the whole rod. In the large AR rods that it is possible to synthesize with the present approach, quantitative HRTEM analysis is less straightforward. Nevertheless, it shows that the CdSe region is rarely localized near the tips of the rods nor at their center, but in most cases in a region between $^1/_3$ and $^1/_4$ of their overall length (see Supporting Information). This is consistent with a fast growth rate of the rods along the unique *c*-axis of their wurtzite structure, the growth along one direction of this axis being faster than along the opposite direction, as observed previously[3] and also as predicted theoretically for wurtzite-type nanorods.[22] An additional advantage of the present synthetic approach is that it yields rods that have few structural defects, as can be inferred by the low density of stacking faults along the rod structure.

Optical absorption and photoluminescence (PL) spectra of CdSe/CdS nanorods in solution show a considerable red-shift with respect to the corresponding spectra of the starting CdSe seeds (Figure 3a,b). In samples of large AR rods, the absorption spectra are characterized by well-resolved peaks appearing at higher energies with respect to the lowest energy peak (Figure 3a). Theoretical absorption spectra (Figure 3a, dashed lines) were calculated using the envelope function approximation[23] (see also Supporting Information). The nanorods were modeled as a CdSe sphere inside a CdS hexagonal prism. The three-dimensional single-band effective mass Hamiltonian was solved on a Cartesian grid, using the parameters taken from Müller et al.[24] (i.e. $m_e = 0.13$, $m_h = 0.45$, for CdSe; $m_e = 0.2$, $m_h = 0.70$ for CdS; zero conduction band-offset) and bulk energy gaps at room temperature from Landolt−Börnstein[25] (i.e., 1.75 eV for CdSe and 2.5 eV for CdS). The theoretical absorption spectrum shown in Figure 3a is obtained by considering transitions in the single-particle approximation from the highest 50 hole levels to the lowest 50 electron levels and applying a Gaussian broadening ($\sigma = 50$ meV) to each exciton level. The calculated spectra are in good agreement with the experimental data. On the basis of the results of the calculations, the high-energy peaks in the absorption spectra can be ascribed to the absorption from CdS, while the lowest energy peak is due to electronic transitions from holes confined in the CdSe core to electrons delocalized throughout the whole nanocrystal structure as a consequence of the negligible conduction band offset between CdSe and CdS.[26] This

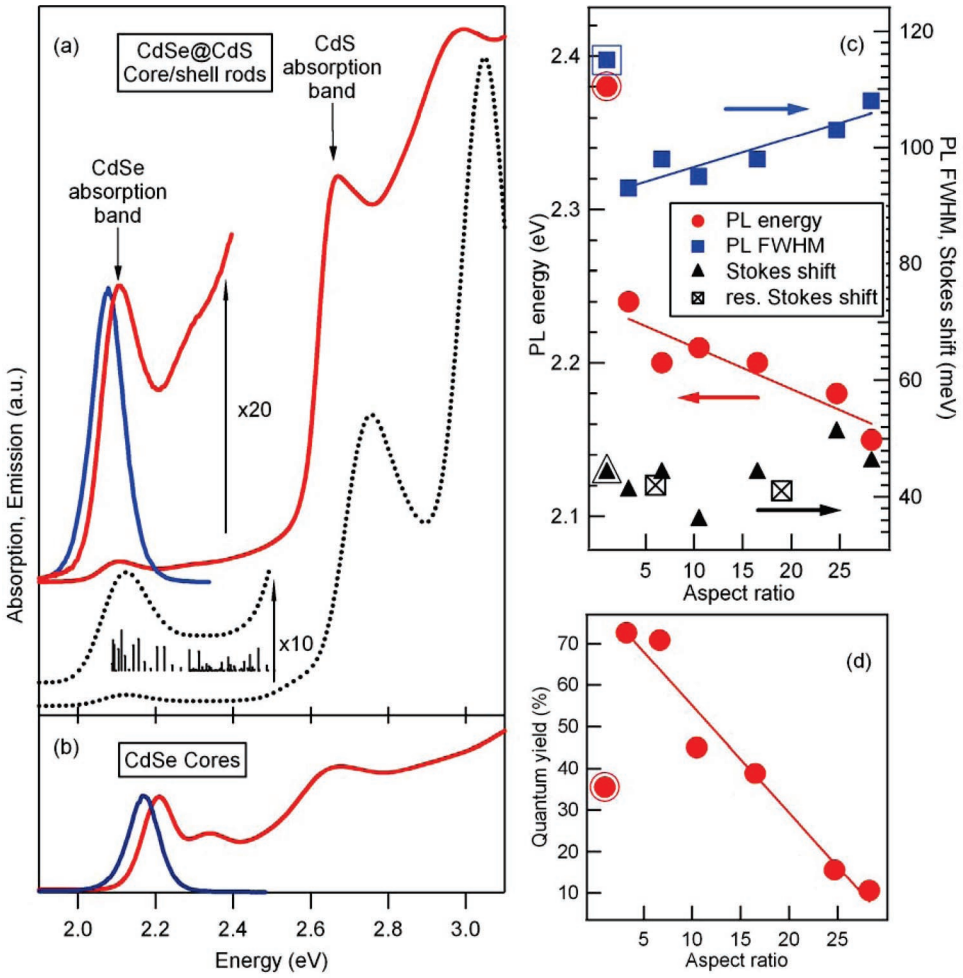

Figure 3. Measured and modeled optical parameters of CdSe/CdS nanorods. (a) Optical absorption and photoluminescence (PL) spectra of a typical sample of CdSe/CdS nanorods dissolved in toluene (continuous lines). The rods have an average length of 51 nm and average diameter of 3.9 nm. They were prepared from CdSe seeds with a diameter of 3.2 nm. The corresponding theoretical absorption spectrum is shown in dotted lines.[23] Vertical bars in the ×10 magnification of the low-energy side of calculated spectrum indicate the energy position and oscillator strength of the first few exciton levels, which represent transitions from the hole 1S level of the CdSe sphere to the electron nS levels of the CdS rod. The absorption and PL spectra of the starting spherical CdSe nanocrystal sample are shown in (b). Spectra of core−shell samples show always a considerable red-shift with respect to the corresponding spectra of the starting CdSe seeds. (c) Nonresonant Stokes shifts (labeled "Stokes shift" in the legend), full width at half-maximum, and PL peak energy for different samples of CdSe/CdS nanorods prepared from the same batch of CdSe seeds (which had a diameter of 2.3 nm). The corresponding values of the starting CdSe seeds are indicated by outlined markers, and the resonant Stokes shifts obtained from PLE experiments at $T = 10$ K are indicated with crossed box markers. In going from the nanorods with the smallest AR to those with the largest AR, the average diameter of the rods varies from 3.5 to 5 nm, and their average length varies from 10 to 130 nm, respectively. Straight lines are inserted as a guide to the eye. (d) Quantum yields of the same nanorods samples as in (c).

behavior has been already observed in both spherical and asymmetric core−shell CdSe/CdS nanocrystals but grown at much lower temperatures (120−150 °C).[19,26]

The full widths at half-maximum of the PL peaks for all our rods remain relatively narrow even in large AR rods (Figure 3c) and therefore are indicative of the high homogeneity in shape of our samples and of the limited occurrence of graded composition (a graded shell) at the CdSe/CdS core−shell interface. Also, it is remarkable that even growth temperatures as high as those at which our nanorods are synthesized (350−380 °C) are not able to cause alloying of the CdSe core with the growing CdS shell, a situation that would lead instead to a blue-shift in the optical absorption and emission spectra of the resulting $CdSe_xS_{1-x}$ alloy nanorods with respect to those of the starting CdSe seeds.[27] The nonresonant Stokes shifts for the nanorods (i.e., shifts between the emission peak and the lowest energy peak in absorption, see plot of Figure 3c) range from 40 to 50 meV and are not much different from those of the starting CdSe seeds. In addition, such shifts show a negligible dependence on the AR of the rods, differently from what had been reported earlier on CdSe/CdS nanorods prepared by Talapin and co-workers at much lower temperatures, for which much bigger and strongly AR-dependent Stokes shifts were observed.[19] Such reduced Stokes shifts confirm the size homogeneity and low interdiffusion of chemical species in our nanostructures. Also resonant Stokes shifts, determined by low-temperature PLE measurements (Figure 3c and

Supporting Information) are not dependent on the AR of the rods, provided that the latter are all prepared starting from the same CdSe seeds.

PL quantum yields (QYs) from core−shell rods in solution are of the order of 70−75% for short AR rods and decay to about 10% in the largest AR rods that we could synthesize (Figure 3d). The relatively high QYs of the short AR nanorod samples, which are comparable to those of spherical or asymmetric core−shell nanocrystals reported earlier,[19,26] point to a homogeneous shell growth, with little presence of defects in the core−shell interfacial region, even under the fast growth rates taking place in our syntheses. For ARs larger than 10, the decrease in QY can be due to an increasing number of surface trap states arising from the CdS region. Such decrease of QY, together with a more delocalized electron wave function (which therefore has a smaller overlap with the hole wave function), results in increased radiative decay times in longer rods (i.e., they vary from 13.5 ns in rods with AR equal 3, to 164 ns in rods with AR equal to 28, see Supporting Information for more details).

The CdSe/CdS nanorods reported here start self-assembling on substrates as soon as the solvent in which they are dissolved is allowed to evaporate, forming long-range ordered assemblies that are reminiscent of liquid-crystalline phases (Figure 1). The formation of these types of assemblies is entropically driven and has been observed already in several colloidal nanorod solutions.[4,11,13,20] Also, ordered arrays of close-packed, vertically aligned nanorods can be obtained by evaporation-mediated self-assembly of nanorods on substrates from more concentrated nanorod solutions. We have observed the formation of small areas of vertically oriented nanorods already when a drop of solution is deposited on the carbon support film of TEM grids, similar to those seen by Li and Alivisatos.[14] However, larger areas, often of the order of several square micrometers, can be achieved when the process is carried out on the surface of water.[7] As an example, we let the solvent evaporate from a concentrated solution of nanocrystals in toluene that had been deposited on the surface of water in a glass beaker, and we then collected part of the floating nanocrystal film with a carbon-coated TEM grid. Some regions of this film are shown in Figure 4a−c. Regular patterns of vertically stacked nanorods are seen, which are organized either in hexagonally close-packed monolayers (Figure 4b) or in ordered multilayer structures (Figure 4a, bottom right, and Figure 4c). In general, interfacial self-segregation of nanoparticles leads to a reduction of interfacial energy, and for instance, the segregation of TOPO-coated spherical CdSe nanocrystals at the water−toluene interface has been observed recently.[28] It is likely that vertical assembly of nanorods in our experiments leads to a lower interfacial energy than for a lateral close-packed or disordered assembly at the interface, as in this configuration each nanorod has one of its polar facets (which are also less passivated with surfactants than its nonpolar facets and are likely to carry residual charges) closer to the water−toluene interface. In addition, such arrangement maximizes the hydrophobic interactions among nanorods, at least in monolayer structures. Evaporation-mediated assembly on warm (50−60 °C) water led to the most reproducible results, as higher temperature improves rod solubility and should help the system to reach such lower energy configuration, in analogy with the conditions recently found for the formation of complex binary superlattices of spherical nanoparticles.[29]

We also observed the formation of large vertically aligned nanorod arrays when the evaporation-mediated assembly took place on TEM grids that had been placed on electrostatically charged surfaces or, with a higher degree of control, by using planar electrodes separated by some tens of micrometers distance (see Figure 4d). For the latter experiments, we used silicon nitride membrane window grids with a nitride thickness of 100 nm on which we evaporated a 10 nm Ti gate from the back side for the vertical alignment of nanorods. A standard carbon-coated TEM grid placed on top of the membrane during solvent evaporation served as a counter electrode. We used a voltage of 32 V, while the nanorod solution and its container were heated to 45 °C. Also, in this case, we find that temperature has a significant influence on the alignment because, under the same conditions, but with solution and container at 20 °C (instead of 45 °C for successful vertical alignment), we observed mainly lateral alignment in ribbon structures (see Figure 4e) and only few and very small areas of vertically aligned rods. We attribute the dominant driving forces for this alignment to a combination of the interaction of the rods with the electric field via their intrinsic dipoles,[7,30] and thermal effects like conductivity and convective flow of the liquid in the evaporation process.[14] A similar degree of assembly could not be achieved for instance with CdS-only rods or with CdSe rods prepared by any of the synthetic routes reported so far, most likely because of their comparatively broader size distributions.

Also the lateral alignment of nanorods can be extended over larger areas and controlled in direction if the evaporation-mediated assembly is influenced by an external perturbation like an electric field.[7−10] As an example, we exploited the presence of a significant dipole in this type of nanorods[30] to laterally align them on planar surfaces using external electric fields. In this case, we used interdigitated electrode devices (electrode separation 4 μm, electrode length 600 μm), which were fabricated by optical lithography and subsequent metal evaporation (500 nm Al) on Si/SiO_2 (100 nm oxide thickness) substrates. A quantity of typically 50 μL of nanorod solution (nanorods were dispersed in toluene, the optical density of the solution at 595 nm was equal to 0.05) was drop-casted onto the electrode device under ambient conditions, and a dc electric field of 2.5 10^5 V/cm was applied during solvent evaporation (typically 2 min). After the alignment process, the electrode devices were inspected by scanning electron microscopy (SEM) imaging. The rods aligned uniformly over areas on the scale of several tens of square micrometers by following the field streamlines throughout the electrode gap (Figure 5a and Supporting Information). Magnifications of randomly picked areas in between the electrodes showed indeed an almost perfect lateral alignment of rods in monolayers or multilayered

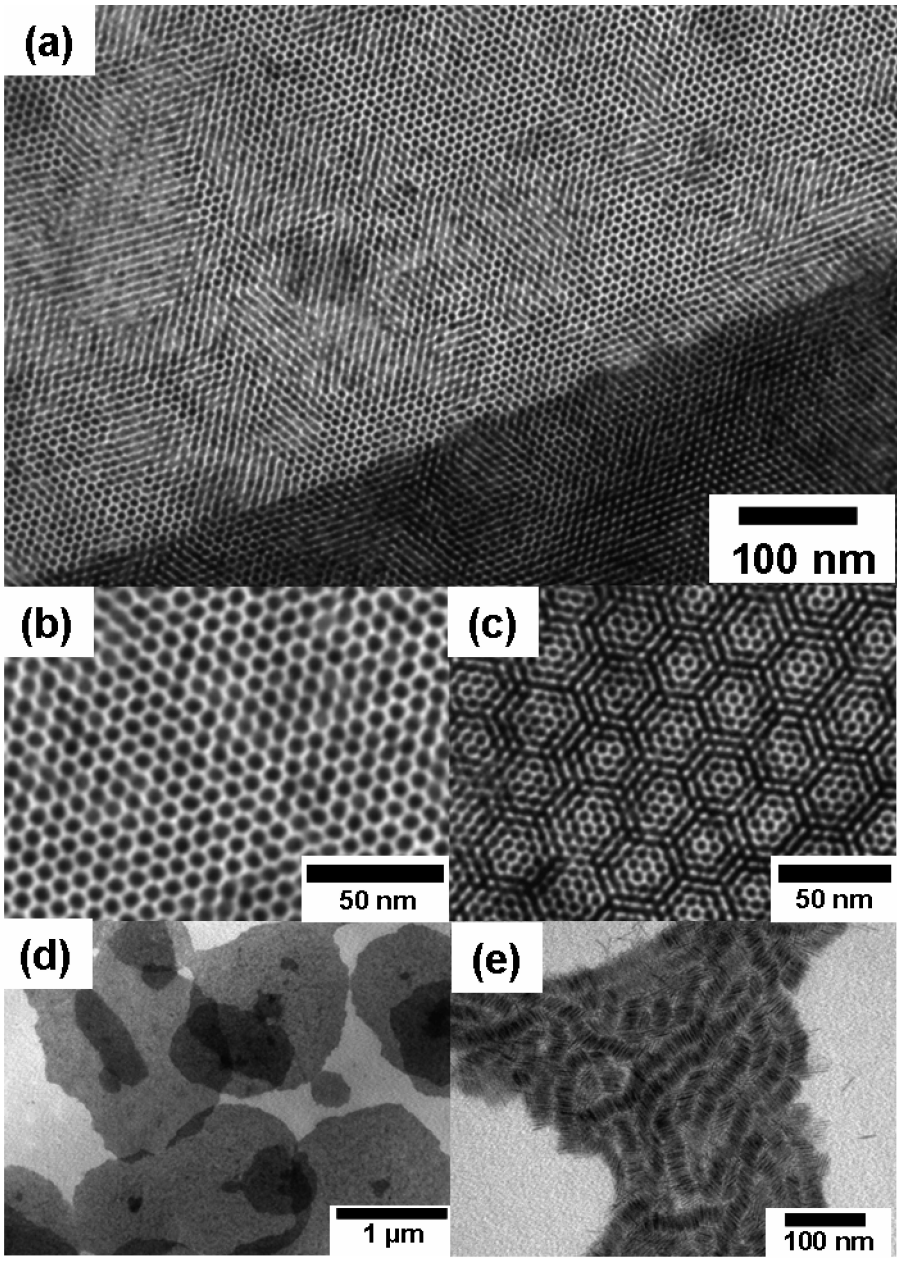

Figure 4. TEM images of ordered nanorod arrays obtained by evaporation-mediated self-assembly. (a) Micrometer size closely packed layers of vertically stacked rods obtained upon evaporation of toluene on top of water. (b−c) Higher magnification imaging revealed regular patterns of vertically stacked nanorods, which are organized either in hexagonally closed packed monolayers (b) or in multilayer structures (a, bottom right, and c). (d) Micrometer size plaques of vertically aligned rods obtained by an electric field in vertical direction. (e) Lateral ribbon structures that consist of a few multilayers of nanorods.

structures, with a type of organization that resembles either the nematic (Figure 5b) or the smectic liquid-crystal phases (Figure 5c). The polarized emission from the regions of aligned nanorods under ambient conditions was recorded with a conventional microphotoluminescence setup. The sample was excited by a circularly polarized He−Cd laser at 325 nm. The emitted light was collected by a objective lens (20× magnification, NA = 0.4) and detected by a 0.33 m monochromator equipped with an Andor CCD camera. The emission polarization was analyzed with a linear polarizer in combination with a λ-half plate, placed in front of the monochromator to correct the polarization-dependent response of both the monochromator and the detector (see illustration in Figure 4d). Figure 5d(ii) shows the fluorescence emission spectra recorded from a micrometer size region of aligned nanorods under ambient conditions. The PL of such large arrays of oriented nanorods is strongly polarized along the alignment direction. The integrated PL intensity dependence on the polarizer angle can be fitted nicely to a $\cos^2$ function as shown in Figure 5 d(iii). Polarization ratios as high as 45% were observed on such micrometer size oriented ensembles for rods that had an AR of 10. As a control experiment, we performed the same measurements after rotating the sample by 90° and obtained the same results shifted by 90°. Also, control experiments performed on

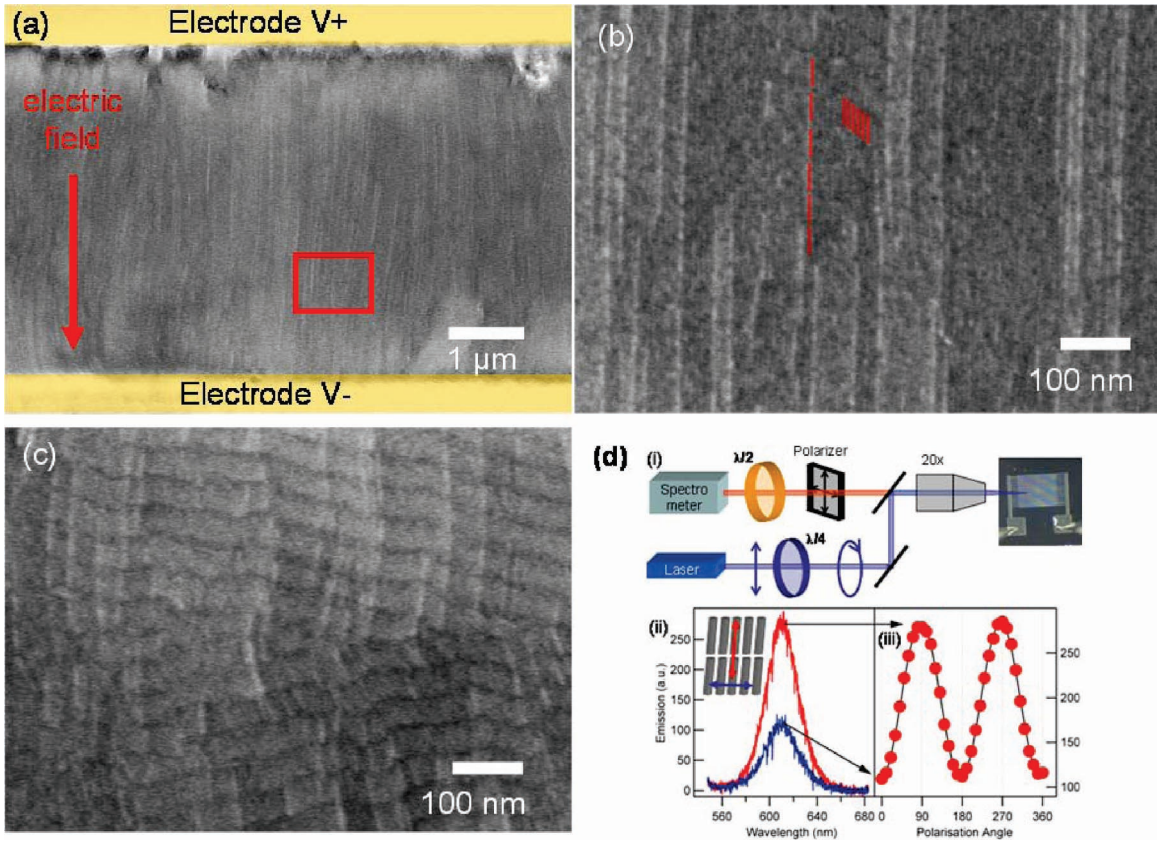

Figure 5. Lateral alignment of nanorods with electric fields and polarized emission from aligned nanorods. (a−c) SEM images showing aligned arrays of nanorods with an aspect ratio of 10. The red arrow indicates the direction of the electric field that was applied during the evaporation of the nanorod solution, and the red square marks the region that is displayed in (b). (b) Micrometer size area where the individual rods can be resolved. Some rods are highlighted in red as a guide to the eye. (c) Zoom that displays an area of nanorods assembled in ribbonlike structures. (d) (i) Schematic illustration of the experimental setup. (ii) Nanorod emission spectra, recorded from the micrometer size regions of aligned nanorods under ambient conditions, polarized parallel (red) and perpendicular (blue) to the long axis of the nanorods, as illustrated by the schematic inset. (iii) Red dots show the PL intensity dependence on the polarization angle and can be fitted to a $\cos^2$ function (black line). From the data a polarization ratio of 45% can be calculated as $(I_{||} - I_{\perp})/(I_{||} + I_{\perp})$. Here, $I_{||}$ and $I_{\perp}$ are the emission intensities parallel and perpendicular to the long axis of the rods, respectively.

regions of randomly oriented nanorods did not show any significant polarization of the fluorescence emission.

Figure 6 shows spatially resolved PL spectra that were collected with a confocal system (Olympus FV1000) in epilayer configuration (with a spatial resolution of 200 nm) from different regions of substrates on which nanorods exhibited the following different types of alignment: densely packed hexagonal arrays of vertically aligned rods, laterally aligned ribbon-like assemblies, and disordered assemblies (see insets of Figure 6). The samples were excited by an UV diode laser ($\lambda = 405$ nm) through an objective lens 60× oil with a numerical aperture of NA = 1.40. The emission from areas with 300−500 nm diameter, which were selected with the confocal system, was detected by a 0.32 m monochromator equipped with a nitrogen-cooled CCD camera that was coupled to the confocal head (the spectral resolution of the whole system is 0.5 nm). The nanorod samples were deposited on a substrate consisting either of a carbon-coated TEM grid or of a 100 nm thick silicon nitride membrane. Measurements on several arrays of nanorods with also different ARs show that the regions of vertically oriented rods are almost nonemissive (Figure 6) and their PL spectrum is slightly blue-shifted with respect to that from areas of disordered nanorods. Areas of ribbonlike assemblies of nanorods are characterized by strong PL emission, which is significantly blue-shifted (up to 30 meV) with respect to the PL from areas of disordered nanorods. The difference in PL intensity between ribbonlike and vertically aligned nanorod arrays could be due to the spatial anisotropy of the optical dipole emission field of elongated nanorods. The emission from such nanocrystals, in which the transition dipole is parallel to the nanorod long axis, is expected to be maximal in the plane perpendicular to the dipole and minimal in the direction of the nanorod long axis. The blue-shift observed in emission could be related to the screening of the internal (piezo)electric field present in each nanorod that is induced by the photogenerated charge distributions in neighboring rods, which should be more efficient in ordered assemblies than in disordered aggregates. Förster resonance energy transfer, which should lead to a red-shift in the PL of close-packed assemblies of nanorods,[31] is not observed here probably due to the nearly monodisperse size distribution of such nanorods. Wave function delocalization and the formation of minibands, which should also cause a red-shift of the PL spectrum,[32] can be theoretically estimated to be

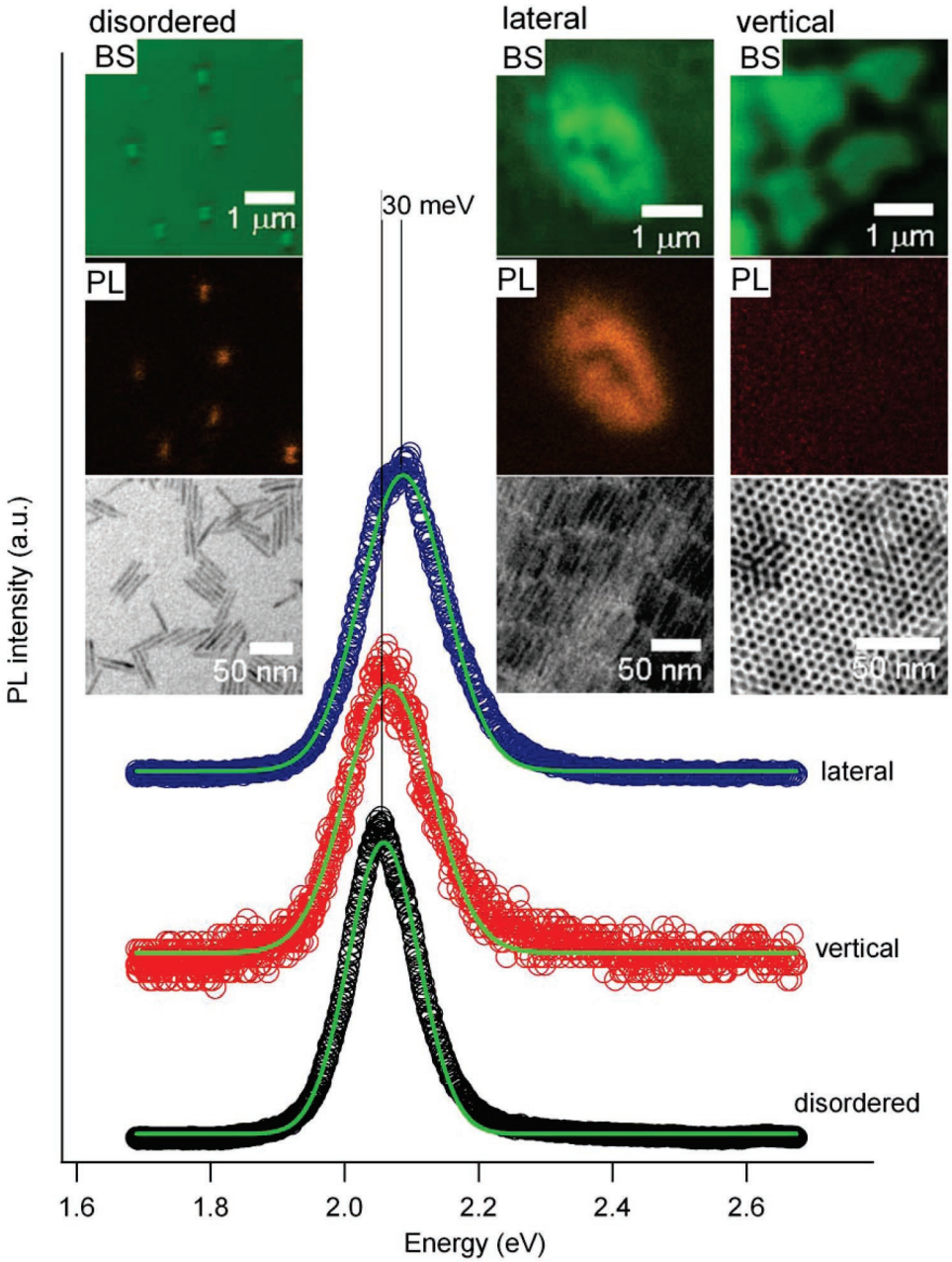

Figure 6. PL from different types of nanorod assemblies. PL spectra of regions of laterally, vertically aligned, and disordered nanorods with AR = 10 are marked by the open circles. The Gaussian fits of the data shown by solid green lines give 2.06, 2.07, and 2.09 eV as energy peak position for disordered ensemble, vertical arrays, and lateral arrays, respectively. The PL spectra were normalized with respect to their amplitude and shifted vertically for clarity. The insets show corresponding images of the laser backscattering (BS) and photoluminescence (PL) intensity of regions consisting of disordered, vertically, and laterally aligned nanorod arrays recorded with the confocal setup, and representative TEM images taken from the respective regions (various regions of self-assembled vertically and laterally aligned nanorods were mapped by inspecting the substrate under low magnification TEM). Large areas of vertically aligned nanorods (with respect to the substrate) were observed that could also be spotted under the confocal microscope, as they showed a characteristic "globular" and often faceted shape (see Figure 4d). The bright areas in the backscattering images originate from the nanorod ensembles.

of the order of 0.7 meV (see Supporting Information) and is therefore negligible.

The ability to fabricate ordered, large-scale assemblies of colloidal semiconductor nanorods as those reported here should strengthen the studies on physical properties arising from superstructure organization and coupling effects among nanorods. Also, it should promote further exploitation of these materials into functional, nanocrystal-based devices such as solar cells, solar concentrators, light-emitting diodes, and field effect transistors. In addition, the seeded-growth method is easily extendible to other combinations of materials, and as a proof of concept, we demonstrate here its viability to the synthesis of tetrapod-shaped ZnTe/CdS and ZnSe/CdS nanocrystals (see Supporting Information). In this case, the starting ZnTe or ZnSe seeds have a cubic zinc-blende structure, which leads to the concerted growth of four CdS arms on top of such seeds. In particular, for the case of ZnTe seeds, the resulting ZnTe/CdS tetrapods too have a

significantly narrow distribution of arm lengths and diameters (see Supporting Information), which should lead to further exploitation also of colloidal nanocrystal tetrapods in self-assembled functional materials and devices.

Acknowledgment. This work was supported by the European projects ESTEEM (contract no. 026019), SA-NANO (contract no. 013698), and NANOTAIL (contract no. 042459), and by the Italian Ministry of Research (contract nos. RBLA03ER38 and RBIN048TSE). We thank Dr. Elvio Carlino and Dr. Davide Cozzoli for useful discussions.

Supporting Information Available: Detailed description of the syntheses of nanorods and tetrapods of various materials by seeded growth, structural analysis on long aspect ratio rods, additional details on electric field alignment of nanorods, theoretical calculations on isolated nanorods and on close-packed, vertically aligned nanorod assemblies, time-resolved optical measurements, and low-temperature PLE measurements. This material is available free of charge via the Internet at http://pubs.acs.org.

References

(1) Hao, E.; Schatz, G. C.; Hupp, J. T. *J. Fluoresc.* **2004**, *14*, 331−341.
(2) Jun, Y. W.; Lee, J. H.; Choi, J. S.; Cheon, J. *J. Phys. Chem. B* **2005**, *109*, 14795−14806.
(3) Kumar, S.; Nann, T. *Small* **2006**, *2*, 316−329.
(4) Jana, N. R. *Angew. Chem., Int. Ed.* **2004**, *43*, 1536−1540.
(5) Ghezelbash, A.; Koo; Koergel, B. A. *Nano Lett.* **2006**, *6*, 1832−1836.
(6) Harnack, O.; Pacholski, C.; Weller, H.; Yasuda, A.; Wessels, J. M. *Nano Lett.* **2003**, *3*, 1097−1101.
(7) Ryan, K. M.; Mastroianni, A.; Stancil, K. A.; Liu, H. T.; Alivisatos, A. P. *Nano Lett.* **2006**, *6*, 1479−1482.
(8) Gupta, S.; Zhang, Q.; Emrick, T.; Russell, T. P. *Nano Lett.* **2006**, *6*, 2066−2069.
(9) Hu, Z.; Fischbein, M. D.; Querner, C.; Drndić, M. *Nano Lett.* **2006**, *6*, 2585−2591.
(10) Nobile, C.; Fonoberov, V. A.; Kudera, S.; Della Torre, A.; Ruffino, A.; Chilla, G.; Kipp, T.; Heitmann, D.; Manna, L.; Cingolani, R.; Balandin, A. A.; Krahne, R. *Nano Lett.* **2007**, *7*, 476−479.
(11) Li, L. S.; Walda, J.; Manna, L.; Alivisatos, A. P. *Nano Lett.* **2002**, *2*, 557−560.
(12) Dumestre, F.; Chaudret, B.; Amiens, C.; Respaud, M.; Fejes, P.; Renaud, P.; Zurcher, P. *Angew. Chem., Int. Ed.* **2003**, *42*, 5213−5216.
(13) Talapin, D. V.; Shevchenko, E. V.; Murray, C. B.; Kornowski, A.; Forster, S.; Weller, H. *J. Am. Chem. Soc.* **2004**, *126*, 12984−12988.
(14) Li, L. S.; Alivisatos, A. P. *Adv. Mater.* **2003**, *15* (5), 408−411.
(15) Sun, B. Q.; Sirringhaus, H. *J. Am. Chem. Soc.* **2006**, *128*, 16231−16237.
(16) Kim, F.; Kwan, S.; Akana, J.; Yang, P. D. *J. Am. Chem. Soc.* **2001**, *123*, 4360−4361.
(17) Artemyev, M.; Moller, B.; Woggon, U. *Nano Lett.* **2003**, *3*, 509−512.
(18) Markov, I. V. *Crystal Growth for Beginners: Fundamentals of Nucleation, Crystal Growth, and Epitaxy*; World Scientific: Singapore, 2003.
(19) Talapin, D. V.; Koeppe, R.; Gotzinger, S.; Kornowski, A.; Lupton, J. M.; Rogach, A. L.; Benson, O.; Feldmann, J.; Weller, H. *Nano Lett.* **2003**, *3*, 1677−1681.
(20) An, K.; Lee, N.; Park, J.; Kim, S. C.; Hwang, Y.; Park, J. G.; Kim, J.-Y.; Park, J.-H.; Han, M. J.; Yu, J.; Hyeon, T. *J. Am. Chem. Soc.* **2006**, *128*, 9753−9760.
(21) GPA Phase plug-in for DigitalMicrograph (Gatan) available from HREM Research Inc.: http://www.hremresearch.com.
(22) Rempel, J. Y.; Trout, B. L.; Bawendi, M. G.; Jensen, K. F. *J. Phys. Chem. B* **2005**, *109*, 19320−19328.
(23) Bastard, G., *Wave Mechanics Applied to Semiconductor Heterostructures*; John Wiley & Sons: New York, 1991.
(24) Müller, J.; Lupton, J. M.; Lagoudakis, P. G.; Schindler, F.; Koeppe, R.; Rogach, A. L.; Feldmann, J.; Talapin, D. V.; Weller, H. *Nano Lett.* **2005**, *5*, 2044−2049.
(25) *Landolt-Börnstein, New Series, Group III, Vol. 17b*; Springer: New York, 1982.
(26) Peng, X. G.; Schlamp, M. C.; Kadavanich, A. V.; Alivisatos, A. P. *J. Am. Chem. Soc.* **1997**, *119* , 7019−7029.
(27) Swafford, L. A.; Weigand, L. A.; Bowers, M. J.; McBride, J. R.; Rapaport, J. L.; Watt, T. L.; Dixit, S. K.; Feldman, L. C.; Rosenthal, S. J. *J. Am. Chem. Soc.* **2006**, *128*, 12299−12306.
(28) Lin, Y.; Skaff, H.; Emrick, T.; Dinsmore, A. D.; Russell, T. P. *Science* **2003**, *299*, 226−229.
(29) Shevchenko, E. V.; Talapin, D. V.; O'Brien, S.; Murray, C. B. *J. Am. Chem. Soc.* **2005**, *127*, 8741−8747.
(30) Li, L. S.; Alivisatos, A. P. *Phys. Rev. Lett.* **2003**, *90*, 097402.
(31) Kagan, C. R.; Murray, C. B.; Bawendi, M. G. *Phys. Rev. B* **1996**, *54*, 8633−8643.
(32) Artemyev, M. V.; Woggon, U.; Jaschinski, H.; Gurinovich, L. I.; Gaponenko, S. V. *J. Phys. Chem. B* **2000**, *104*, 11617−11621.

NL0717661